– Electronic Supplementary Information (ESI) –

Unraveling Structural and Magnetic Information during Growth of Nanocrystalline $SrFe_{12}O_{19}$

Cecilia Granados-Miralles,[1] Matilde Saura-Múzquiz,[1] Espen D. Bøjesen,[1] Kirsten M. Ø. Jensen,[2] Henrik L. Andersen[1] & Mogens Christensen[1]*

[1] *Center for Materials Crystallography CMC, Department of Chemistry & iNano, Aarhus University, Denmark*

[2] *Nanoscience Center, Department of Chemistry, University of Copenhagen, Denmark*

**e-mail corresponding author: mch@chem.au.dk*

CONTENTS

IN SITU EXPERIMENTS

Temperature calibration

For both experimental setups, there is a small offset between the setpoint of the heating device and the actual temperature felt by the sample. A temperature calibration was done on the sapphire tube/spiral reactor filled with deionized water and pressurized up to 250 bars. The temperature inside the tube/spiral was measured with a type K thermocouple.

For the in situ setup, the temperature was measured for 4 different setpoints: 250, 300, 350 and 400°C. The obtained heating curves are shown in black color in Figure 3 in the article. The temperature reaches its maximum value after about 20 seconds in all cases. Figure S 1 shows a plot of the temperature measured after 180 seconds vs. the heat gun setpoints, which follows a linear trend. The actual temperature at which the reported experiments took place was simply interpolated from that linear regression.

The temperature inside the spiral reactor (*ex situ* setup) was only measured for the working temperature. A temperature of 243 °C was reached when the set point was 240 °C.

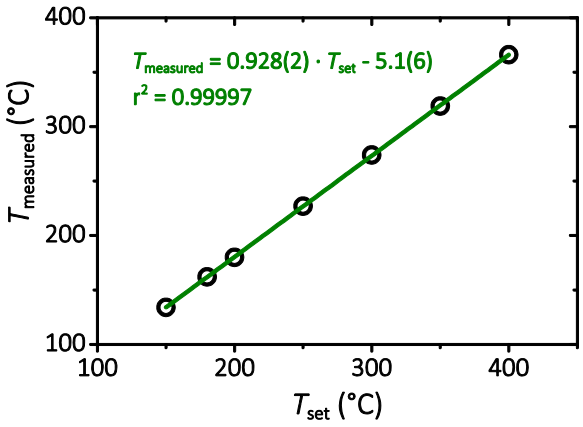

Figure S 1. Temperature calibration for the *in situ* experimental setup.

Synchrotron PXRD data reduction: azimuthal integration and instrumental resolution

Synchrotron powder X-ray diffraction data were collected as two-dimensional images. Figure S 2(a) is an example of the raw 2D-data collected. To allow subsequent Rietveld analysis of the data, these images were integrated to one-dimensional 2θ-scans, as the one shown in Figure S 2(b) The mentioned task was carried out using the software *Fit2D*[1]. First, accurate values for sample-to-detector distance and detector tilt (in and out-of-plane) are obtained from a standard powder (LaB_6 NIST 660b) packed in a 0.3 mm glass capillary and measured in the exact same experimental configuration as the samples. Later, those values were used for integration of the datasets of the hydrothermal experiments. Detector count statistics and normalization of the background throughout all the frames of the same experiment was carried out with a purpose written MATLAB script. Figure 4 in the article shows a complete time-resolved dataset after all these corrections.

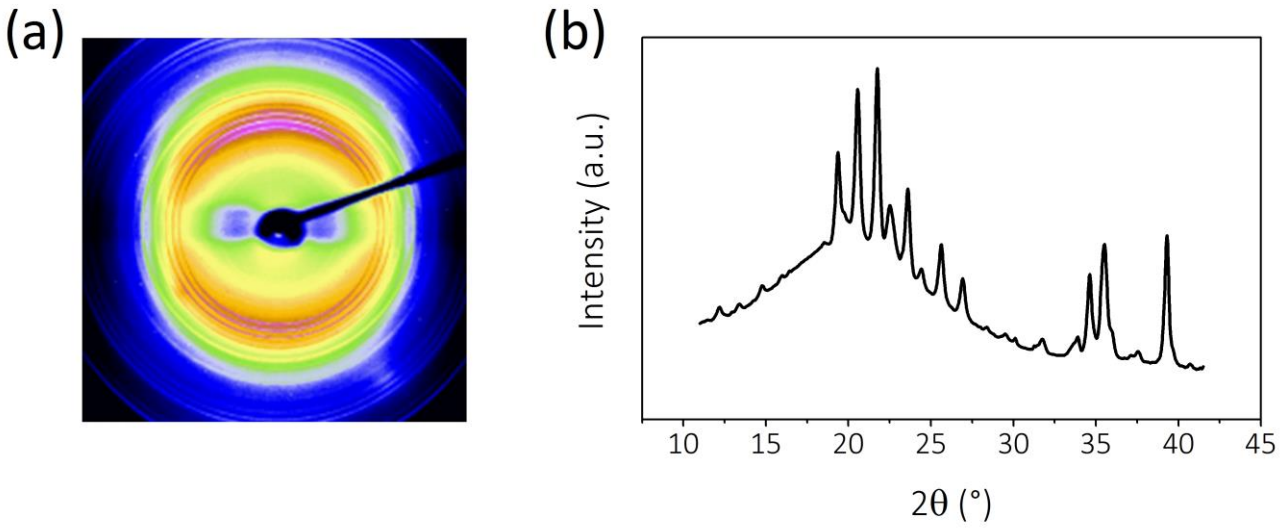

Figure S 2. (a) Example of raw powder X-ray diffraction 2D-data collected in 5 seconds. (b) 2θ-scan obtained after azimuthal integration with *Fit2D*.

– Electronic Supplementary Information (ESI) –

Sequential Rietveld refinements for *in situ* synchrotron PXRD data

Further data treatment is necessary for a quantitative analysis. Rietveld analysis of the diffraction data was performed using the suite of programs *FullProf*[2]. First, a good model for the well-formed final product is achieved (long reaction times). Later, the program is run sequentially towards the beginning of the experiment (short times). A new model for each data frame is readily found by refining the model achieved for the previous one.

Table S I summarizes the refined parameters and R-values for the *in situ* experiment conducted at 245 °C and a reaction time of 4 min, when $SrFe_{12}O_{19}$ and the six-line phase coexist.

Table S I. Refined parameters for the *in situ* data collected after 4 min of reaction at 245 °C. $SrFe_{12}O_{19}$ and the six-line coexist at that stage of the experiment.

Phase	Weight Fraction (%)	Crystallite Size (nm)		Unit Cell Parameter (Å)		R_f	R_{wp}	X^2
		a/b-plane	*c*-axis	a=b	c			
$SrFe_{12}O_{19}$	35(1)	20(2)	6.0(4)	5.8929(7)	23.184(8)	5.13	13.5	0.381
$Fe_{0.86}OO$	65(3)	19.9(1)	7.3(4)	2.9374(2)	9.303(2)	2.27		

Six line ferrihydrite: description of the phase

The description of the FeOOH was based in the defect-free structure published by Jansen *et al.*[3] However, the z-coordinate and the site occupation for the iron atom were refined to significantly different values. Table S II shows the refined values for the sample reacted during 20 seconds in the spiral reactor. These values were kept constant for all the other samples described in the article.

Table S II. Crystallographic description of the six-line FeOOH.

Atom	Atomic coordinates			Wyckoff position	Occupancy
	x	y	z		
O^{2-}	0	0	0	2b	100%
Fe^{3+}	1/3	2/3	0.14493(6)	4f	43.08(2)%
O^{2-}	2/3	1/3	1/4	2d	100%

In situ hydrothermal synthesis with an Fe/Sr ratio of 12

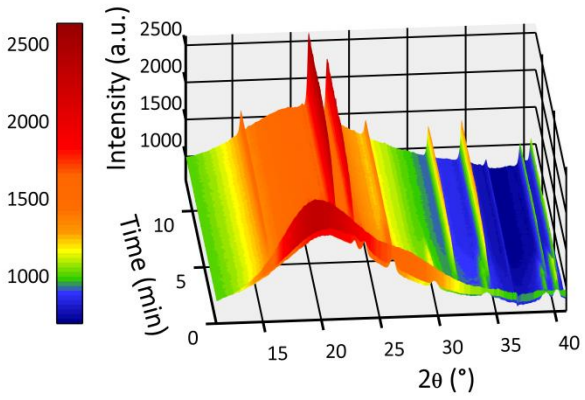

Figure S 3. *In situ* experiment at approx. 320 °C using an Fe/Sr ratio of 12. Initially FeOOH is formed. It readily transforms into pure hematite (α-Fe_2O_3).

Crystallite growth kinetics: Johnson–Mehl–Avrami–Kolmogorov model

The Johnson–Mehl–Avrami–Kolmogorov (JMAK) model was used to extract information about the kinetics of the process. Although this model was originally developed for solidification and recrystallization of metals, it has often been applied before to similar systems.[4,5]

Following the procedure described by Andersen *et al.*[6] the time-resolved data for $SrFe_{12}O_{19}$ were fitted to the expression $f(t) = 1 - e^{-(k[t-t_0])^n}$, where $f(t)$ is the extent of the reaction, k is the rate constant, t_0 is the induction time, and n is the Avrami exponent. The fits for the datasets at the four different temperatures are shown in Figure S 4(a).

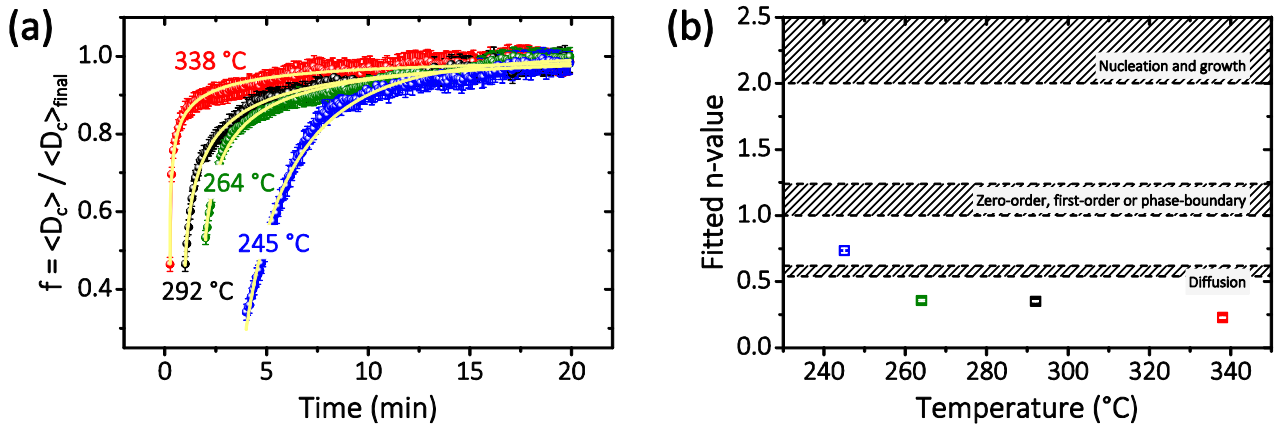

Figure S 4. Extent of the reaction fitted with the JMAK model. (b) Fitted values of the Avrami exponent.

To avoid the intensity fluctuations of the synchrotron beam to interfere with the observations, Andersen *et al.* chose to define the extent of the reaction using the crystallite volume instead of the scale factor or the integrated intensity of a single peak. In the present study, the crystallite size is known with accuracy only along one dimension of the platelets, *i.e.*, the thickness $<D_c>$. As explained in the manuscript, the diameter of the platelets $<D_a>$ is beyond the resolution limit of the experiment. For that reason, it is not possible to accurately calculate the crystallite volume in our case so the extent of the reaction was defined in terms of the platelets thickness $f(t)$ is defined as $f(t) = <\boldsymbol{D_c}>(\boldsymbol{t})/<\boldsymbol{D_c}>_{final}$, instead of using the crystallite volume as it is done in the mentioned reference. Therefore, the conclusions extracted from applying the JMAK model in this

case will only refer to the growth in thickness of the platelets. This approximation very likely implies loss of relevant information, since previous studies have shown that the crystallite growth of $SrFe_{12}O_{19}$ is different along the two dimensions.[7] However, it is the best the data allowed in this case.

The fitted values for the Avrami exponents n are plotted in Figure S 4(b). The obtained values suggest that the reaction mechanisms at the three higher temperatures (264, 292 and 338 °C) are essentially limited by the diffusion process, while at the lowest temperature (245 °C) phase-boundaries seem to play a role too.

EX SITU EXPERIMENTS

Background description on Rietveld refinements of the *ex situ* data collected for short reaction times

For the short reaction times (20 s, 40 s and 1 min), the background could not be described with a Chebyshev polynomial alone. The major obstacle was the fact that the (110) and (220) reflections from SFO are already perceptible for the sample reacted for as short time as 20 s, but at the same time the crystallinity of the aforementioned compound was still not sufficiently evolved to resolve the characteristic diffraction peaks. Therefore, this feature cannot really be fully described neither by a smooth polynomial function nor a crystalline phase.

The strategy we implemented to overcome this setback was exploiting the fact that scattering from an amorphous phase is essentially the same phenomenon as diffraction from very nanosized crystals. In both cases, a lack of vast long-range order regions is preventing the non-constructive interferences (away from the Bragg condition) from cancelling one another. This effect taken to the extreme is very close to the case of the amorphous phase.

This X-ray amorphous $SrFe_{12}O_{19}$ contribution to the background was modelled as a LeBail fit, while the background itself was fixed to a straight line with an optimized slope and y-intercept. As an example, the final model for the sample reacted for 20 seconds is shown in Figure S5. With this type of fitting, free oscillation of intensities is allowed until an energy minimum is reached. The size and shape parameters of the crystallites of this phase were fixed to very small values, especially along the *c*-direction. The platelets were defined to have an approximate diameter of 5 unit cells and the thickness corresponding to about a third of the unit cell value along the *c*-direction. It must be emphasized that the procedure described above is only intended to be a means of achieving a proper description of the background and so being able to model the data, but no structural information was extracted from this “background phase”.

For reaction times longer than 1 min, a regular Chebyshev polynomial was used to describe the background (see Figure S6). In this case, we attribute this none-flat background to some water present in the samples. Due to their high hygroscopy, oxide nanoparticles tend to attract water molecules from the surrounding and hold them onto their surface. The smaller the particles, the more hygroscopic they are. Thereby, 13 coefficients were required to achieve a proper description in the 2 min sample, while 6 coefficients were used for 5 min and only 4 were needed for both 10 min and 20 min.

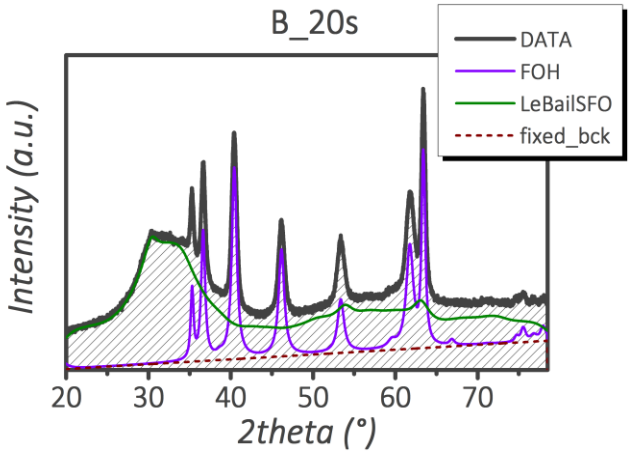

Figure S5. Deconvolution of the different contributions to the final Rietveld model proposed for short reaction times (sample 20s).

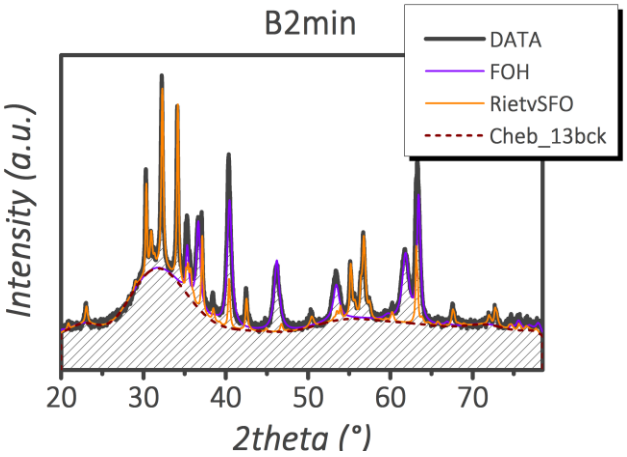

Figure S6. Deconvolution of the different contributions to the final Rietveld model proposed for reaction times greater than 1 min (sample 2 min).

Calculation of the magnetic figures of merit

The magnetic moment *m* (measured in emu) is divided by the sample mass to obtain the mass magnetization *M* in emu/g. The magnetization is converted to SI units using the relation

$$M_{mass}\left(\frac{Am^2}{kg}\right) = M_{mass}\left(\frac{emu}{g}\right)$$

The magnetic field is measured in Oe and converted to SI units as

$$H_{app}\left(\frac{kA}{m}\right) = \frac{H_{app}(Oe)}{4\pi}$$

The magnetic field is corrected for demagnetization using

$$H_{eff}\left(\frac{kA}{m}\right) = H_{app}\left(\frac{kA}{m}\right) - NM_{vol}\left(\frac{kA}{m}\right)$$

where H_{app} is the applied magnetic field, N is the demagnetizing factor and M_{vol} is the volume magnetization at the corresponding H_{app}. M_{vol} is calculated multiplying M_{mass} times the density in g/cm^3. A demagnetizing factor of $N = 0.33$ was used.

M_s is the mass magnetization value for an applied field of 2 T. M_r is determined graphically as the y-intercept in a plot of the magnetization M versus the effective magnetic field H_{eff} as done in Figure 10 in the article. H_c is also determined graphically from the x-intercept.

The energy product *BH* is calculated using the equation

$$BH\left(\frac{kJ}{m^3}\right) = \mu_0\left(H_{eff} + M_{vol}\right) * H_{eff}$$

where $\mu_0 = 4\pi * 10^{-4}\frac{V\,s}{kA\,m}$ and H_{eff} and M_{vol} are introduced in kA/m.

BH_{max} is the maximum value of the *BH* product in the second quadrant of the hysteresis loop.

Spatially-resolved EDS elemental analysis

There seems to be a consistent tendency for less Sr in the smaller particles but no definitive conclusion can be extracted, very likely due to Sr being present in an amorphous form.

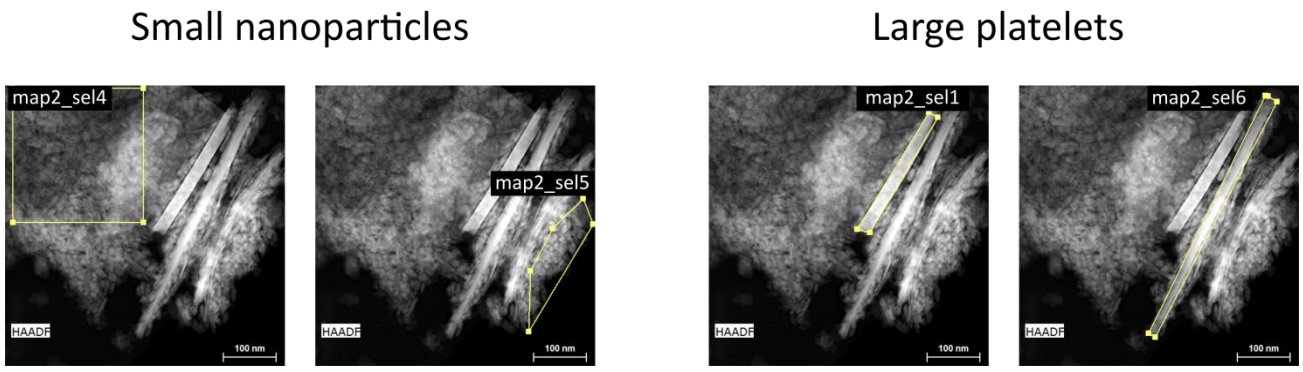

Figure S7. Spatially resolved elemental analysis of sample 2 min.

Table SIII. Atomic percentages calculated from the EDS spectra of the selected regions of the image (small nanoparticles).

	Sr	Fe	O
Theor. $Fe_{0.86}OO$	0	30.07	69.93
map2_sel4	2.30	32.89	64.81
map2_sel5	2.24	32.63	65.13

Table SIV. Atomic percentages calculated from the EDS spectra of the selected regions of the image (large platelets).

	Sr	Fe	O
Theor. $SrFe_{12}O_{19}$	3.13	37.5	59.38
map2_sel1	3.70	36.13	60.16
map2_sel6	3.47	34.70	61.83

References

1 A. P. Hammersley, S. O. Svensson, M. Hanfland, A. N. Fitch and D. Hausermann, *High Press. Res.*, 1996, **14**, 235–248.

2 J. Rodríguez-Carvajal, *Phys. B Condens. Matter*, 1993, **192**, 55–69.

3 E. Jansen, A. Kyek, W. Schäfer and U. Schwertmann, *Appl. Phys. A Mater. Sci. Process.*, 2002, **74**, s1004–s1006.

4 R. J. Francis and D. O'Hare, *J. Chem. Soc. Dalt. Trans.*, 1998, 3133–3148.

5 K. M. Ø. Jensen, C. Tyrsted, M. Bremholm and B. B. Iversen, *ChemSusChem*, 2014, **7**, 1594–1611.

6 H. L. Andersen, K. M. Ø. Jensen, C. Tyrsted, E. D. Bøjesen and M. Christensen, *Cryst. Growth Des.*, 2014, **14**, 1307–1313.

7 M. Saura-Múzquiz, C. Granados-Miralles, M. Stingaciu, E. D. Bøjesen, Q. Li, J. Song, M. Dong, E. Eikeland and M. Christensen, *Nanoscale*, 2016, **8**, 2857–2866.